Concept Paper

Comparison of Experimental and Simulated Separation Performance in Capillary Tube-in-Manifold Devices

Christopher Piccolo[1], Michael Keller[2], Daniel J. Czarnecki[3], Thomas Austin[2], Graham Shelver[2], and James P. Grinias[1,*]

[1]Department of Chemistry & Biochemistry, Rowan University, Glassboro, NJ 08028

[2]IDEX Health & Science, Rohnert Park, CA 94928

[3]IDEX Health & Science, Bristol, CT 06010

*Corresponding Author: James P. Grinias, grinias@rowan.edu

Keywords: Liquid Chromatography; Column Preparation; Microfluidics; Computational Fluid Dynamics

Abstract

A metal tube-in-manifold packed bed capillary column device, designed to overcome common limitations associated with capillary LC separations is described. Experimental results of initial packing tests with sub-3 μm core-shell particles demonstrated efficiencies greater than 47,000 plates/m for a separation performed using the column device. Computational fluid dynamics (CFD) modeling of the multicomponent separation used for this work was validated against experimental LC results and the optimized model was able to effectively predict component peak retention times. However, the accuracy of predicted efficiencies requires further

refinement. The tube-in-manifold design demonstrates that packed capillary columns with cylindrical cross-sectional channel geometry and ultrahigh pressure, low dead volume fluidic connections are achievable.

1. Introduction

The increase in efficiency observed in liquid chromatographic separations over the past several decades has typically focused on decreasing particle diameter and increasing system pressure limits [1–3]. However, challenges exist in exceeding current instrument limits of 1500 bar using traditional analytical-scale columns [4,5]. As pressures increase at high flow rates, viscous heating occurs which can reduce chromatographic efficiency due to the formation of radial thermal gradients. To achieve significantly higher pressures, accommodating longer columns packed with smaller diameter particles, the use of capillary columns with smaller inner diameters (i.d.'s) is most effective at minimizing the effects of these radial thermal gradients [6,7]. However, this can lead to new challenges in instrument design, as the smaller volume capillary columns can be more susceptible to extra-column broadening effects related to injectors, connecting tubing, and detectors [8,9]. One approach that can overcome both obstacles is the use of integrated microfluidic LC devices that closely couple sample introduction, the separation column, and detection with minimal dead volume [10–14].

Several approaches to designing microfluidic LC columns have been described, including packed particle beds [15], monolithic columns [16,17], and pillar arrays [18]. To access the widest range of commercially available chromatographic separation modes, packed particle beds are most desirable because the same stationary phases can be readily employed in the microfluidic column channels. The biggest disadvantage to this approach is that particle packed

beds typically have the highest flow resistance of these column types, requiring "world-to-chip" connections with high pressure limits in order to connect other instrument components. Previously reported commercial options for fitting-based connections had pressure limits in the 150-690 bar range [19], while literature reports have demonstrated 500 bar limits for glass chips [19] and pressures exceeding 1500 bar for titanium chips [20,21]. This latter description provides a workable range that can fully utilize the current limits of commercial UHPLC pumps, although it requires specialized fittings and precision setting of the connections to avoid excess dead volume [21].

In this concept report, we explore the use of a new metal-based microfluidic packed bed column format that is compatible with modern face-sealing tubing connections that are now commonplace within UHPLC instrumentation [22]. The design and format of the device are described and a separation achieved by packing the channel with sub-3 μm core-shell particles [23–25] is demonstrated. Progress towards computational fluid dynamics (CFD) modeling [26] to describe the separation performance that is observed experimentally and help inform future manifold designs is also presented.

2. Materials & Methods

2.1. Manifold Design and Manufacturing

A schematic drawing of the capillary tube-in-manifold device is shown in **Figure 1**. To fabricate the devices, a length of stainless steel tubing (grade 304, 27-gauge, regular wall – 0.0163" [410 μm] outer diameter (o.d.) x 0.0083" [210 μm] inner diameter (i.d.)) is placed within a channel in a 316 stainless-steel supporting structure which includes bend radii greater than ten times the i.d. of the tube. The tube is affixed within the channel-containing substrate

using a combination of Marine epoxy 314 resin with 102 hardener (TAP Plastics, San Leandro, CA) and mechanical fasteners. In combination with a backplate of the same substrate material to the primary manifold layer, the fasteners and epoxy firmly clamp and enclose the tubing in place. This supports the internal tubing that contains the separation channel and ensures mechanical strength and stability. A cross-sectional image of the tubing following the bonding of these layers is shown in **Figure 1B**. The epoxy is only used to support the tubing in place and does not actually come in contact with any mobile phase solvents. Extra tubing beyond the surface of the manifold is then cut approximately flush and the entire surface is smoothed using a lapping process. Counterbores for accepting inlet and outlet frits were placed at the inlet and outlet ports of the tubing by post-bond machining using traditional machining techniques (**Figure 1C**). Finally, removable fitting ports with #10-32 UNF-2B internal threads designed for MarvelXACT tubing with integrated fittings (IDEX Health & Science, Oak Harbor, WA) were attached above the inlet and outlet holes using #6-32 UNC-2B machine screws. These removable fitting ports are aligned to the inlet and outlet ports using precision 1/8" diameter dowel pins and corresponding holes to ensure good fluid path alignment. **Figure 1D** shows a photograph of the fully integrated manifold device.

2.2. Column Preparation and Characterization

A capillary tube-in-manifold device containing a 0.2 x 150 mm channel (**Figure 1A**), was packed with Halo C_{18} 2.7 μm 160 Å core-shell particles (Advanced Materials Technology, Wilmington, DE). A 25 mg/mL particle slurry in 1:1 acetone:acetonitrile (both HiPerSolv HPLC grade, VWR, Radnor, PA) was sonicated for 10 minutes and then loaded into a high pressure packing reservoir (**Figure S1**) that was connected to the inlet of the manifold device. Acetone

was also used as a pushing solvent for packing, which was initiated at 150 bar using a DSHF-300 Haskel pump (Burbank, CA). The packing pressure was increased to 1000 bar until the channel was filled and then pressure was slowly released to minimize disruptions to the packed bed. The 0.018" diameter inlet and outlet frits consisted of 0.015" thick Bekipor ST 3AL3 stainless steel mesh (Bekaert, Marietta, GA). The mesh was manually inserted into the counterbored holes in the manifold (**Figure 1C**) using a custom tool (**Figure 2A**). A magnified image of one of these frits cut and inserted is shown in **Figure 2B**.

Chromatographic efficiency was tested using an alkylphenone test mix consisting of thiourea (Acros Organics, Morris Plains, NJ), acetophenone (Alfa Aesar, Ward Hill, MA), propiophenone (Acros Organics, Morris Plains, NJ), and butyrophenone (Alfa Aesar, Ward Hill, MA) at a concentration of 300 ppm (w/w) with the mobile phase as the diluent. The mobile phase consisted of 55% acetonitrile in water (both HiPerSolv HPLC grade, VWR, Radnor, PA) with 0.1% trifluoroacetic acid (Sigma-Aldrich, Saint Louis, MO). Tests were performed at 1.5 µL/min with mobile phase flow generated from a nanoAcquity binary solvent manager (Waters, Milford, MA). The pump was connected to a prototype 104 nL internal sample loop injector which was then connected to the manifold channel inlet with a 0.025 x 100 mm Marvel XACT connecting tube. Valve actuation was timed at 0.1 s to provide an approximate minimal injection volume of 2.5 nL at the operating flow rate [8]. The column outlet was connected to a capillary-scale LED-UV absorbance detector module described in [27] (Axcend LLC, Provo UT) with a 0.025 x 100 mm Marvel XACT tube coupled to a 0.025 x 50 mm PEEKsil tube (Trajan Scientific, Ringwood, Australia) using a P-882 adapter (IDEX Health & Science, Oak Harbor, WA) required because of different tubing outer diameters. Data were acquired using a home-built Raspberry Pi data acquisition platform [28] and raw chromatograms were corrected for high

frequency noise with a digital frequency filter and baseline drift with a polynomial fit background subtraction. Retention times and plate counts (also referred to as the total number of theoretical plates, *N*) were calculated using an iterative statistical moments (ISM) algorithm [29] in Igor Pro 6.0 (Wavemetrics, Inc., Lake Oswego, OR). This program was also used for plotting chromatograms.

2.3. CFD Simulation of Separation Performance

A CFD model incorporating Darcian flow, column wall effects with differential stationary phase porosity, sub-optimal fluid path geometries, operating backpressure, and the injection of parameterized analyte, was constructed using the Darcian flow and transport of diluted species in porous media modules of the COMSOL Multiphysics 6.2 simulation tool (COMSOL Inc., Burlington, MA). A model that incorporated flow rate, porosity, analyte concentration, and retention time was developed and tested on cylindrical straight tube and wide radius curve tube geometries. The input variables are listed in **Table S1**. Estimates for diffusion coefficients were made using the Wilke-Chang equation with approximations made for the association constant of acetonitrile based on the mobile phase used in this study [30]. The optimized model was then validated against experimental LC results obtained using the tube-in-manifold device (**Figure 1**) with respect to retention time, plate count, and skew using the same ISM algorithm.

3. Results & Discussion

The capillary tube-in-manifold device (**Figure 1**) consists of a stainless steel tube of a given dimension sealed within a stainless steel manifold body that contains support structures to guide the tube inlet and outlet to the surface, where face-sealing internal thread fittings can be

affixed to accommodate connecting tubing into and out of the device. This approach enables cylindrical packing channels, which provide the highest cross-sectional symmetry and reduce on-column band broadening [31]. Other approaches to achieving cylindrical channels for microfluidic LC columns have required difficult alignment techniques (glass devices) [32] or have had limited pressure ranges (embossed cyclic olefin copolymer devices) [33], both of which are resolved with this design approach.

When preparing packed chromatographic beds in microfluidic devices, it is critical to effectively design a particle retaining frit to ensure packed bed stability. Retaining structures [34] or weirs [35] can be fabricated into the device, monolithic structures [36] or particles [32] can be placed at the end of the separation channel, or a filter material can be placed at the outlet and held in place using connecting tubing [20]. With the capillary tube-in-manifold devices described here, a frit insertion approach enables the use of traditional stainless steel frit material placed within the counterbored connection ports into and out of the separation channel (**Figure 1C**). An insertion alignment tool (**Figure 2A**) enables direct placement of the bulk frit material above the port, with the material inserted into the port using a fine point punch with applied manual pressure. This approach permits particle bed stability with use of a material that is more closely associated with traditional analytical scale columns than the aforementioned approaches to trapping particles in microfluidic LC packed bed columns.

Preliminary efficiency tests of chromatographic beds prepared within the capillary tube-in-manifold device were conducted to test general column performance with a generic packing protocol and provide an empirical comparison to aid in the development of CFD simulations of chromatographic separations using the devices. Experimental conditions were selected to provide a retention factor around 5 for the most retained peak (butyrophenone) and then efficiency of this

peak was measured at a mobile phase flow rate of 1.5 μL/min (observed as approximate van Deemter minimum). In the experimental chromatogram shown in **Figure 3**, the plate count for the butyrophenone peak was 7090 (**Table S2**), which correlates with a plate height of 21 μm (reduced plate height of 7.8). To further improve efficiency, the use of smaller diameter particles and optimized packing procedures utilizing higher pressures [20,21] will be explored in future development of this column platform.

By using the chromatographic data, observed backpressure at the given flow rate and mobile phase composition, and approximate estimates of stationary phase surface area and particle porosities, the replication of the chromatographic separation *in silico* using CFD simulation was pursued. Results from 3D simulation runs (**Figure S2**), showed that the symmetrical wide radius tube-in-manifold design produced minimal flow gradients around each bend (approximately 6% difference between inner and outer wall). Comparison of simulated chromatographic results in the radial bend channel with those from equivalent straight tube geometry (**Figure 3**) indicated less than ~2% difference in retention time and plate count for the three retained analyte peaks (**Table S2**). Compared to the simulated models, the experimental data demonstrated lower plate counts for the unretained void time marker and higher plate counts for the retained peaks, especially propiophenone and butyrophenone, which were both more than double the *in silico* values. Furthermore, the experimental data had more positive skew values than the CFD peaks, designating higher tailing; some of the simulated peaks even demonstrated negative skew (fronting). Based on the conditions used, it is unlikely that column overloading is the cause of this observation and rather may be indicative of the impact of the interparticle porosity values used in the simulation for bulk and wall regions. These values may not effectively lead to the true flow velocities observed in a packed bed, which are typically far more

complex [37] than can be characterized with the current CFD model. The retention time predictions between the CFD and experimental results were much closer (all less than 6% difference) based on optimization of the Langmuir Adsorption coefficient used in the simulation (**Table S1**). These observations indicate that further refinement of the model is needed to fully predict the peak shape of the experimental results, most likely to better take into account extra-column effects based on the observed trends. With improved correlation between the CFD and experimental results, the ability to better predict efficiency trends with different tube geometries that could be used for different integrated column functions can be explored prior to fabrication and experimental testing, thus decreasing overall development cycle times.

4. Conclusions & Future Directions

In this concept study, a new capillary tube-in-manifold platform for LC separations was described. With this design, microfluidic LC columns with cylindrical cross-sectional channels and ultrahigh pressure world-to-chip fluidic connections using face-sealing fittings are achievable. Within the connection ports, robust stainless steel frits can be readily placed to retain particles within the chromatographic bed using materials similar to most commercial columns. Experimental results of initial packing tests demonstrated efficiencies in excess of 47,000 plates/m (for retained butyrophenone peak). CFD modeling of the separation could effectively predict retention times, although further refinement is needed to improve the accuracy of the observed efficiency. From this concept of the column portion of a manifold, continued work will focus on further integration of LC system components, such as an injector and/or a detector, towards a platform that allows for capillary-scale separations at ultrahigh pressures with minimal extra-column volumes.

Declaration of Interests Statement

M.K., D. J. C., T. A., and G.S. are employed by IDEX Health & Science, which is the assignee for patents related to the technology described in this work. Partial funding from IDEX Health & Science in support of this project was provided to C.P. and J.P.G. (Rowan University).

Acknowledgements

This work was supported by the Chemical Measurement and Imaging Program in the National Science Foundation Division of Chemistry under Grant CHE-2045023 (to J.P.G.).

References

[1] F. Gritti, G. Guiochon, The current revolution in column technology: How it began, where is it going?, J. Chromatogr. A. 1228 (2012) 2–19. https://doi.org/10.1016/j.chroma.2011.07.014.

[2] R.E. Majors, Historical Developments in HPLC and UHPLC Column Technology : The Past 25 Years, LC-GC North Am. 33 (2015) 818–840.

[3] K. Broeckhoven, G. Desmet, Advances and Innovations in Liquid Chromatography Stationary Phase Supports, Anal. Chem. 93 (2021) 257–272. https://doi.org/10.1021/acs.analchem.0c04466.

[4] R.E. Majors, Future Needs of HPLC and UHPLC Column Technology, LC-GC Eur. 28 (2015) 658–665. http://www.chromatographyonline.com/future-needs-hplc-and-uhplc-column-technology-0.

[5] K. Broeckhoven, G. Desmet, Advances and Challenges in Extremely High-Pressure Liquid Chromatography in Current and Future Analytical Scale Column Formats, Anal. Chem. 92 (2020) 554–560. https://doi.org/10.1021/acs.analchem.9b04278.

[6] J.W. Jorgenson, Capillary liquid chromatography at ultrahigh pressures, Annu. Rev. Anal. Chem. 3 (2010) 129–150. https://doi.org/10.1146/annurev.anchem.1.031207.113014.

[7] L.E. Blue, E.G. Franklin, J.M. Godinho, J.P. Grinias, K.M. Grinias, D.B. Lunn, S.M. Moore, Recent advances in capillary ultrahigh pressure liquid chromatography, J. Chromatogr. A. 1523 (2017) 17–39. https://doi.org/10.1016/j.chroma.2017.05.039.

[8] J.P. Grinias, B. Bunner, M. Gilar, J.W. Jorgenson, Measurement and Modeling of Extra-

Column Effects Due to Injection and Connections in Capillary Liquid Chromatography, Chromatography. 2 (2015) 669–690. https://doi.org/10.3390/chromatography2040669.

[9] G. Desmet, K. Broeckhoven, Extra-column band broadening effects in contemporary liquid chromatography: Causes and solutions, TrAC Trends Anal. Chem. 119 (2019) 115619. https://doi.org/10.1016/j.trac.2019.115619.

[10] J.P. Grinias, R.T. Kennedy, Advances in and prospects of microchip liquid chromatography, TrAC - Trends Anal. Chem. 81 (2016) 110–117. https://doi.org/10.1016/j.trac.2015.08.002.

[11] D.A. Vargas Medina, E.V.S. Maciel, F.M. Lanças, Miniaturization of liquid chromatography coupled to mass spectrometry. 3. Achievements on chip-based LC–MS devices, TrAC - Trends Anal. Chem. 131 (2020) 116003. https://doi.org/10.1016/j.trac.2020.116003.

[12] C.G. Warren, P.K. Dasgupta, Liquid phase detection in the miniature scale. Microfluidic and capillary scale measurement and separation systems. A tutorial review, Anal. Chim. Acta. 1305 (2024) 342507. https://doi.org/10.1016/j.aca.2024.342507.

[13] X. Yuan, R.D. Oleschuk, Advances in Microchip Liquid Chromatography, Anal. Chem. 90 (2018) 283–301. https://doi.org/10.1021/acs.analchem.7b04329.

[14] F. Haghighi, Z. Talebpour, A.S. Nezhad, Towards fully integrated liquid chromatography on a chip: Evolution and evaluation, TrAC - Trends Anal. Chem. 105 (2018) 302–337. https://doi.org/10.1016/j.trac.2018.05.002.

[15] A. Kecskemeti, A. Gaspar, Particle-based liquid chromatographic separations in

microfluidic devices - A review, Anal. Chim. Acta. 1021 (2018) 1–19. https://doi.org/10.1016/j.aca.2018.01.064.

[16] M. Vázquez, B. Paull, Review on recent and advanced applications of monoliths and related porous polymer gels in micro-fluidic devices, Anal. Chim. Acta. 668 (2010) 100–113. https://doi.org/10.1016/j.aca.2010.04.033.

[17] R. Knob, V. Sahore, M. Sonker, A.T. Woolley, Advances in monoliths and related porous materials for microfluidics, Biomicrofluidics. 10 (2016) 032901. https://doi.org/10.1063/1.4948507.

[18] G. Rozing, Micropillar array columns for advancing nanoflow HPLC, Microchem. J. 170 (2021) 106629. https://doi.org/10.1016/j.microc.2021.106629.

[19] C. Lotter, J.J. Heiland, V. Stein, M. Klimkait, M. Queisser, D. Belder, Evaluation of Pressure Stable Chip-to-Tube Fittings Enabling High-Speed Chip-HPLC with Mass Spectrometric Detection, Anal. Chem. 88 (2016) 7481–7486. https://doi.org/10.1021/acs.analchem.6b01907.

[20] M. Gilar, T.S. McDonald, F. Gritti, Experimental evaluation of chromatographic performance of capillary and microfluidic columns with linear or curved channels, J. Chromatogr. A. 1470 (2016) 76–83. https://doi.org/10.1016/j.chroma.2016.10.004.

[21] M. Gilar, T.S. McDonald, F. Gritti, G.T. Roman, J.S. Johnson, B. Bunner, J.D. Michienzi, R.A. Collamati, J.P. Murphy, D.D. Satpute, M.P. Bannon, D. DellaRovere, R.A. Jencks, T.A. Dourdeville, K.E. Fadgen, G.C. Gerhardt, Chromatographic performance of microfluidic liquid chromatography devices: Experimental evaluation of straight versus serpentine packed channels, J. Chromatogr. A. 1533 (2018) 127–135.

https://doi.org/10.1016/j.chroma.2017.12.031.

[22] J.J. Stankovich, F. Gritti, P.G. Stevenson, G. Guiochon, The impact of column connection on band broadening in very high pressure liquid chromatography, J. Sep. Sci. 36 (2013) 2709–2717. https://doi.org/10.1002/jssc.201300175.

[23] G. Guiochon, F. Gritti, Shell particles, trials, tribulations and triumphs, J. Chromatogr. A. 1218 (2011) 1915–1938. https://doi.org/10.1016/j.chroma.2011.01.080.

[24] B. Bobály, J.L. Veuthey, D. Guillarme, S. Fekete, New developments and possibilities of wide-pore superficially porous particle technology applied for the liquid chromatographic analysis of therapeutic proteins, J. Pharm. Biomed. Anal. 158 (2018) 225–235. https://doi.org/10.1016/j.jpba.2018.06.006.

[25] C. Luo, J.J. DeStefano, T.J. Langlois, B.E. Boyes, S.A. Schuster, J.M. Godinho, Fundamental to achieving fast separations with high efficiency: A review of chromatography with superficially porous particles, Biomed. Chromatogr. 35 (2021) e5087. https://doi.org/10.1002/bmc.5087.

[26] Y.X. Wu, C.B. Ching, The theoretical study of the effect of packing heterogeneity on HPLC by computational fluid dynamics, Chromatographia. 56 (2002) 679–686. https://doi.org/10.1007/BF02492468.

[27] S.W. Foster, E.P. Gates, P.A. Peaden, S. V. Calugaru, W.R. West, M.L. Lee, J.P. Grinias, Column selection considerations in compact capillary liquid chromatography, J. Chromatogr. A. 1701 (2023) 464067. https://doi.org/10.1016/j.chroma.2023.464067.

[28] S.W. Foster, M.J. Alirangues, J.A. Naese, E. Constans, J.P. Grinias, A low-cost, open-

source digital stripchart recorder for chromatographic detectors using a Raspberry Pi, J. Chromatogr. A. 1603 (2019) 396–400. https://doi.org/10.1016/j.chroma.2019.03.070.

[29] S. Hsieh, J.W. Jorgenson, Preparation and Evaluation of Slurry-Packed Liquid Chromatography Microcolumns with Inner Diameters from 12 to 33 μm, Anal. Chem. 68 (1996) 1212–1217. https://doi.org/10.1021/ac950682m.

[30] K. Miyabe, Estimation of molecular diffusivity in aqueous solution of acetonitrile by the Wilke-Chang equation, J. Sep. Sci. 34 (2011) 2674–2679. https://doi.org/10.1002/jssc.201100385.

[31] S. Khirevich, A. Höltzel, D. Hlushkou, U. Tallarek, Impact of conduit geometry and bed porosity on flow and dispersion in noncylindrical sphere packings, Anal. Chem. 79 (2007) 9340–9349. https://doi.org/10.1021/ac071428k.

[32] K. Li, W. Hu, Y. Zhou, X. Dou, X. Wang, B. Zhang, G. Guo, Single-particle-frit-based packed columns for microchip chromatographic analysis of neurotransmitters, Talanta. 215 (2020). https://doi.org/10.1016/j.talanta.2020.120896.

[33] L. Mats, G.T.T. Gibson, R.D. Oleschuk, Plastic LC/MS microchip with an embedded microstructured fibre having the dual role of a frit and a nanoelectrospray emitter, Microfluid. Nanofluidics. 16 (2014) 73–81. https://doi.org/10.1007/s10404-013-1221-x.

[34] S. Ehlert, L. Trojer, M. Vollmer, T. Van De Goor, U. Tallarek, Performance of HPLC/MS microchips in isocratic and gradient elutionmodes, J. Mass Spectrom. 45 (2010) 313–320. https://doi.org/10.1002/jms.1719.

[35] A.G. Chambers, J.S. Mellors, W.H. Henley, J.M. Ramsey, Monolithic integration of two-

dimensional liquid chromatography-capillary electrophoresis and electrospray ionization on a microfluidic device, Anal. Chem. 83 (2011) 842–849. https://doi.org/10.1021/ac102437z.

[36] S. Thurmann, L. Mauritz, C. Heck, D. Belder, High-performance liquid chromatography on glass chips using precisely defined porous polymer monoliths as particle retaining elements, J. Chromatogr. A. 1370 (2014) 33–39. https://doi.org/10.1016/j.chroma.2014.10.008.

[37] S. Bruns, J.P. Grinias, L.E. Blue, J.W. Jorgenson, U. Tallarek, Morphology and separation efficiency of low-aspect-ratio capillary ultrahigh pressure liquid chromatography columns, Anal. Chem. 84 (2012) 4496–4503. https://doi.org/10.1021/ac300326k.

Figure Captions

Figure 1. A cross-sectional schematic drawing of the capillary tube-in-manifold device with ports for face-sealing tubing connections into and out of the device is shown in (A). The cross-sectional area of the embedded tubing and the surface counterbore for frit insertion within the tubing are shown in (B) and (C), respectively. A photograph of the device with face-seal fitting installed at the column inlet is shown in (D).

Figure 2. The insertion of frits into the capillary tube-in-manifold device involves use of a centered frit punching device placed over the counterbores (A). Placement of a frit into the counterbore is shown in (B).

Figure 3. CFD simulation of chromatographic separation of test mixture using straight tube (black dotted trace) and curved bend (blue dotted trace) geometries. Experimental chromatogram using the capillary tube-in-manifold device (0.2 x 150 mm) is shown in the red trace. Chromatographic figures of merit calculated using an iterative statistical moments algorithm are shown in **Table S2**.

Figure 1.

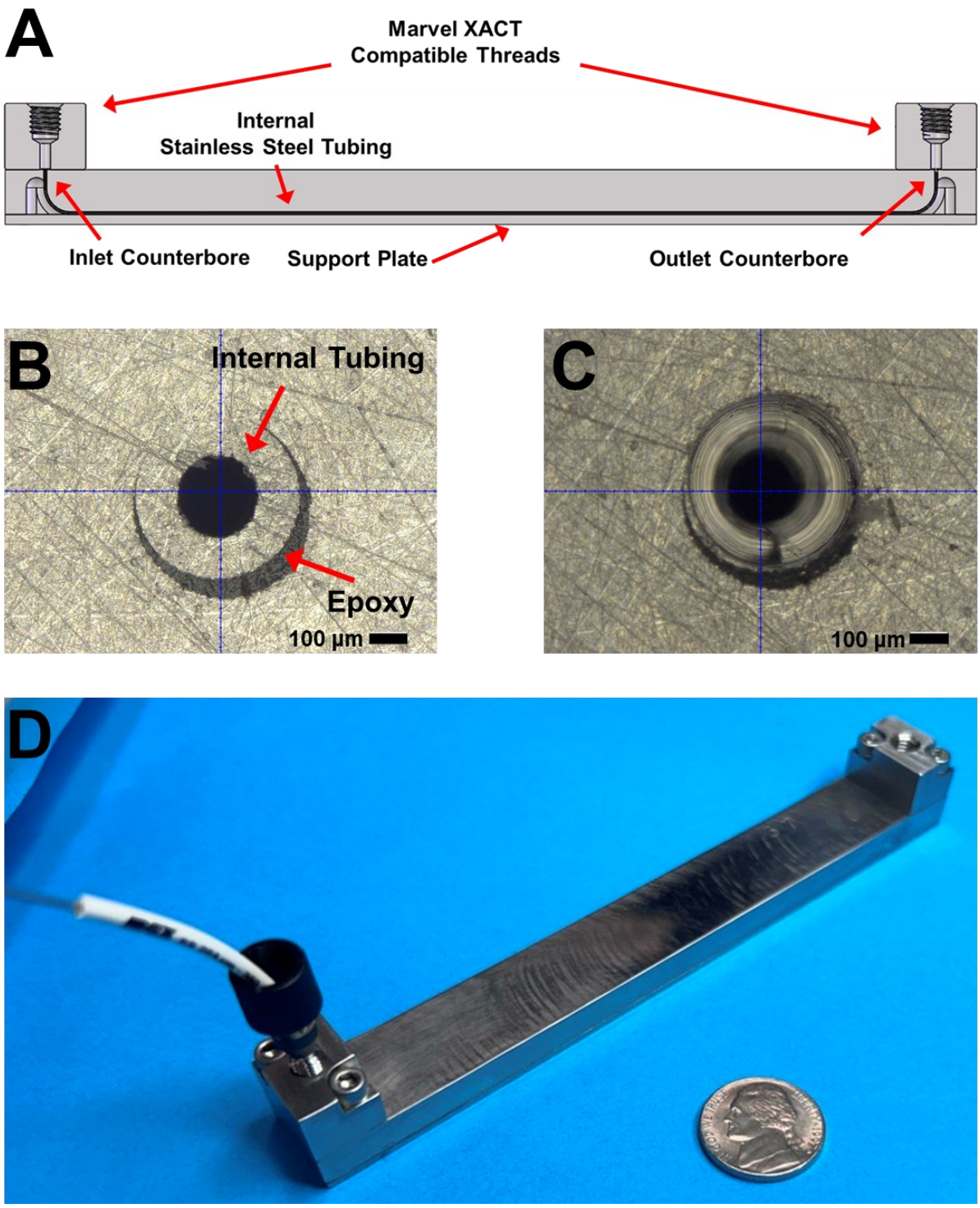
A
Marvel XACT
Compatible Threads
Internal
Stainless Steel Tubing
Inlet Counterbore
Support Plate
Outlet Counterbore
B
Internal Tubing
Epoxy
100 µm
C
100 µm
D

Figure 2.

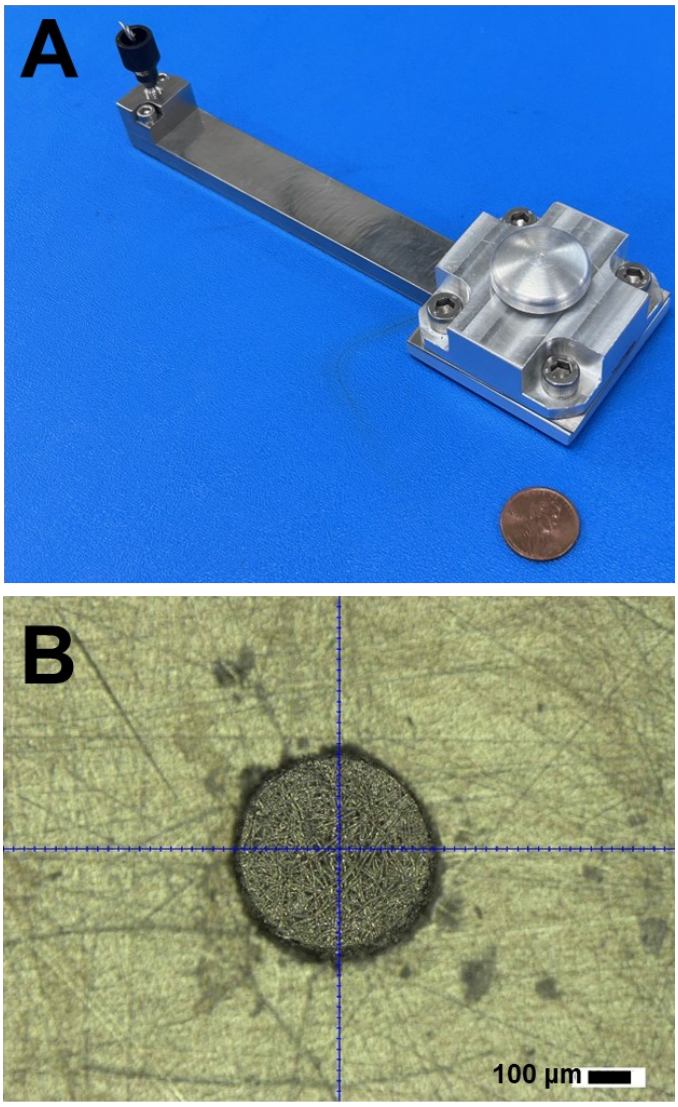

Figure 3.

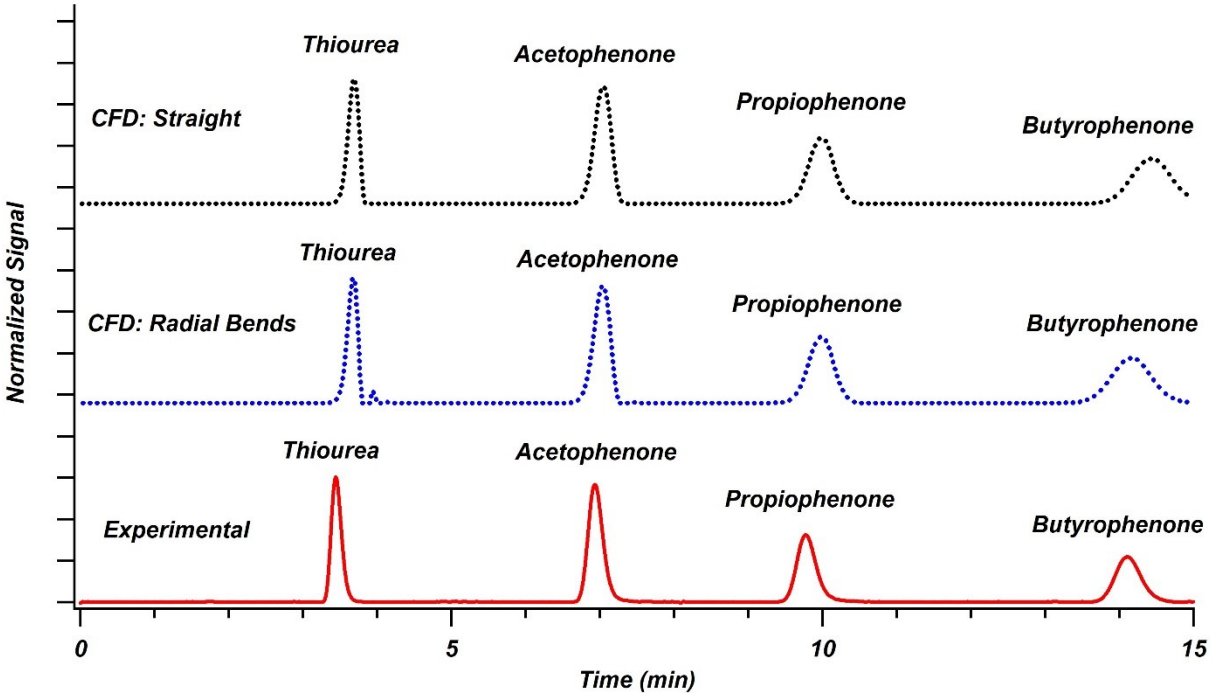
Thiourea
Acetophenone
Propiophenone
Butyrophenone
CFD: Straight
Thiourea
Acetophenone
Propiophenone
Butyrophenone
CFD: Radial Bends
Thiourea
Acetophenone
Propiophenone
Butyrophenone
Experimental
Normalized Signal
0
5
10
15
Time (min)

Concept Paper

Comparison of Experimental and Simulated Separation Performance in Capillary Tube-in-Manifold Devices

Christopher Piccolo[1], Michael Keller[2], Daniel J. Czarnecki[3], Thomas Austin[2], Graham Shelver[2], and James P. Grinias[1,*]

[1]Department of Chemistry & Biochemistry, Rowan University, Glassboro, NJ 08028

[2]IDEX Health & Science, Rohnert Park, CA 94928

[3]IDEX Health & Science, Bristol, CT 06010

*Corresponding Author: James P. Grinias, grinias@rowan.edu

Supporting Information

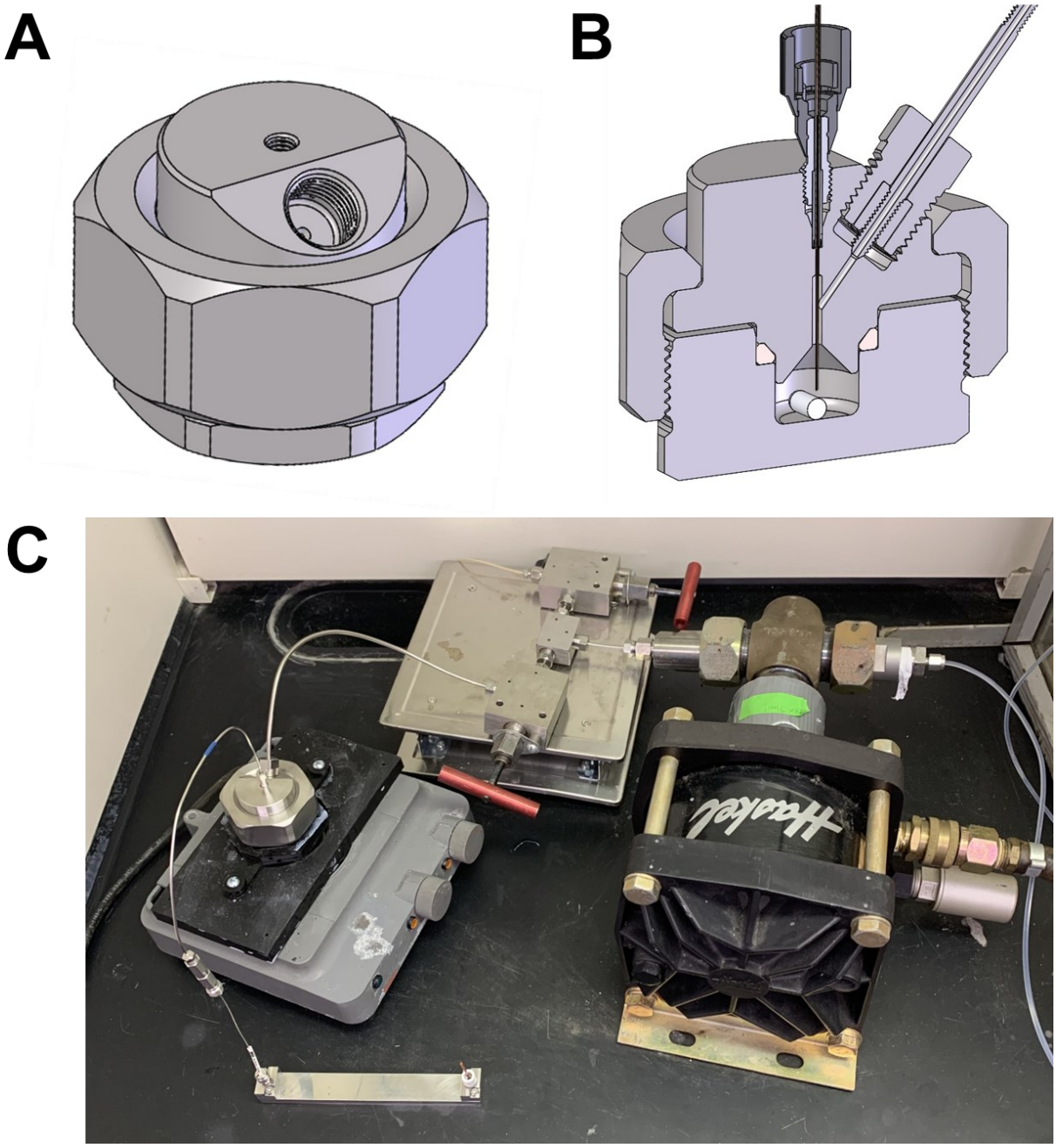

388

389

390 **Figure S1.** External (A) and internal (B) schematic diagrams of the MarvelXACT-compatible
391 slurry packing reservoir. A photograph of the capillary tube-in-manifold device connected to the
392 full column packing apparatus is shown in (C).

393

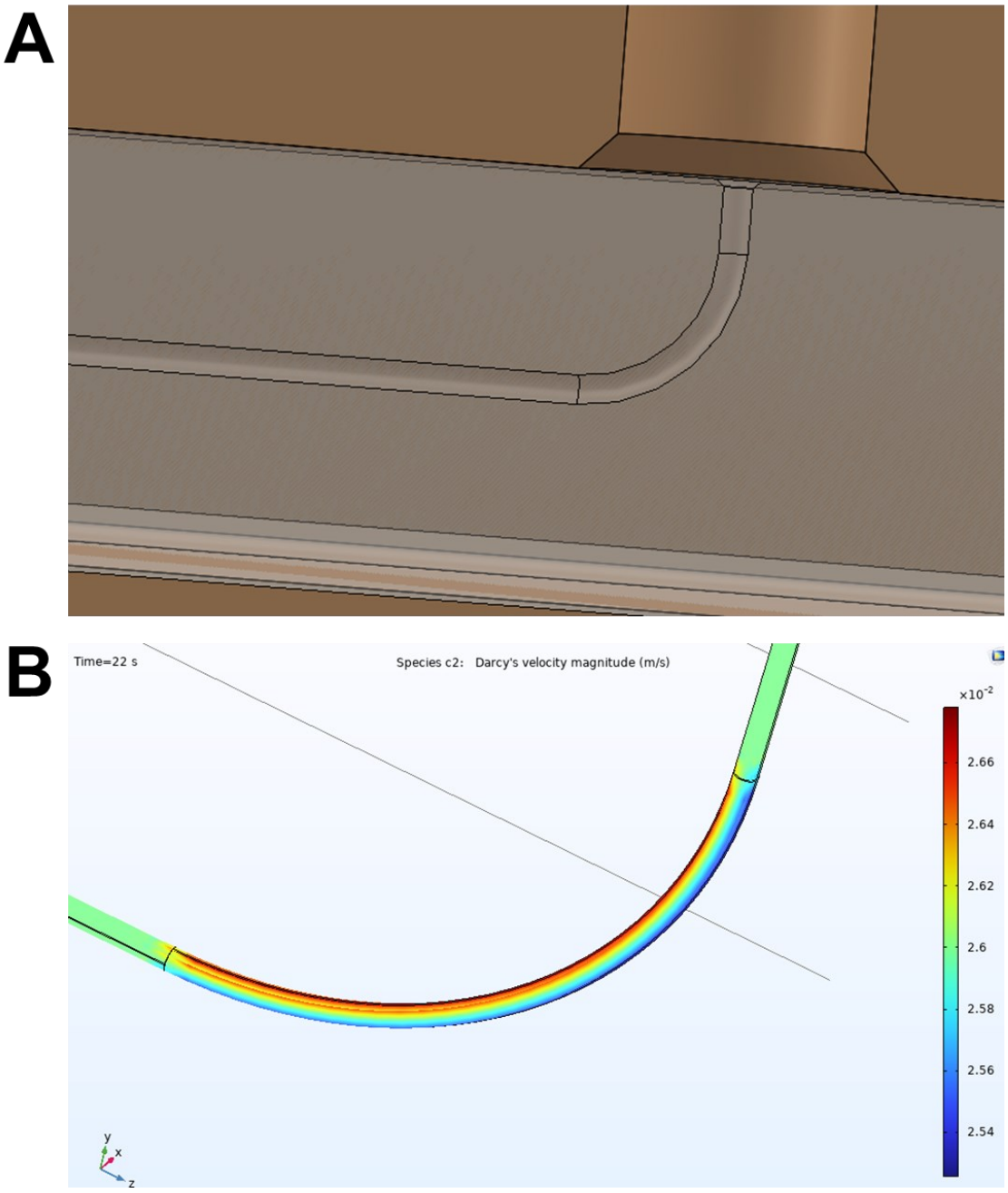

394

395

396 **Figure S2.** Computational reconstruction of radial bend in computational fluid dynamics

397 modeling software (A) and results from flow simulation through packed radial bend (B).

398

399

Table S1. Parameters used in CFD simulation of separation in capillary tube-in-manifold device.

Simulation Parameter	Value
Column length [L_c]	150 mm
Column diameter	200 μm
Particle specific surface area [S]	$1.2e^{5}$ m²/kg
Density solid material particles [rho_p]	2200 kg/m³
Porosity [eps_p]	0.4
Porosity near wall [eps_p2]	0.6
Maximum inlet injector concentration Thiourea	4.468 mol/m³
Maximum inlet injector concentration Acetophenone	2.825 mol/m³
Maximum inlet injector concentration Propiophenone	2.523 mol/m³
Maximum inlet injector concentration Butyrophenone	2.295 mol/m³
Mobile phase linear velocity [v_l]	$4.5e^{-4}$ m/s
Thiourea diffusion coefficient [D_1]	$2.10e^{-9}$ m²/s
Acetophenone diffusion coefficient [D_2]	$1.17e^{-9}$ m²/s
Propiophenone diffusion coefficient [D_3]	$1.07e^{-9}$ m²/s
Butyrophenone diffusion coefficient [D_4]	$9.92e^{-10}$ m²/s
Thiourea Langmuir adsorption constant [K1]	$3.71e^{-4}$ m³/mol
Acetophenone Langmuir adsorption constant [K2]	0.001468 m³/mol
Propiophenone Langmuir adsorption constant [K3]	0.002431 m³/mol
Butyrophenone Langmuir adsorption constant [K4]	0.003793 m³/mol
Monolayer capacity, primary [n01]	$4e^{-6}$ mol/m²

Table S2. Comparison of chromatographic figures of merit (calculated using iterative statistical moments algorithm) for simulated and experimental separations using the capillary tube-in-manifold device.

	Straight Cylindrical Tube (CFD)	**Cylindrical Tube with Two Radial Bends (CFD)**	**Experimental**
Retention Time (min) ***(Thiourea)***	3.67	3.66	3.46
Plate Count ***(Thiourea)***	2880	3340	2770
Skew ***(Thiourea)***	-0.35	-0.44	0.29
Retention Time (min) ***(Acetophenone)***	7.03	7.02	6.95
Plate Count ***(Acetophenone)***	4510	4840	5260
Skew ***(Acetophenone)***	-0.22	-0.34	0.26
Retention Time (min) ***(Propiophenone)***	9.98	9.98	9.80
Plate Count ***(Propiophenone)***	3840	3840	5850
Skew ***(Propiophenone)***	-0.03	-0.05	0.28
Retention Time (min) ***(Butyrophenone)***	14.44	14.17	14.13
Plate Count ***(Butyrophenone)***	3090	3080	7090
Skew ***(Butyrophenone)***	0.05	0.03	0.20